Journal of Magnetic Resonance 347 (2023) 107359

Contents lists available at ScienceDirect

Journal of Magnetic Resonance

journal homepage: www.elsevier.com/locate/jmr

Composite pulse combinations for chirp excitation

Sreya Das *, Navin Khaneja

Systems and Control Engineering Department, Indian Institute of Technology, Bombay, India

ARTICLE INFO

Article history:
Received 5 July 2022
Revised 13 December 2022
Accepted 13 December 2022
Available online 17 December 2022

Keywords:
Broadband excitation
CHORUS
Chirp pulse
Double-refocussing
Composite pulses
Adiabatic pulse

ABSTRACT

Composite pulses are the efficient method for broadband excitation to get control of the limitations of high field NMR, such as resonance offset effects with constraints on rf power that leads to signal intensity distortion. Phase-modulated chirp pulses are used as ordered composite pulse sequences in this paper as **CHORUS** sequence in a high-field NMR spectrometer (BRUKER 750 MHz) for broadband excitation. The composite pulse sequence applies chirp pulses with the forward and the reverse sweep mechanisms. A single excitation pulse combines adiabatic and non-adiabatic rotation, explained as a three-phase rotation, which leaves the magnetizing vectors to a non-uniform phase dispersion as a function of the offset frequency. One adiabatic refocusing pulse of the double sweep rate after the excitation pulse cannot satisfactorily compensate for the phase dispersion. Hence, composite self-refocussing **CHORUS** excitation pulse, with forward, reverse, and their combinations are used to remove the non-uniform phase dispersion generated due to offset resonance frequency. Four such combinations of composite pulses are produced with analytical explanation in this paper. MATLAB simulation results and experimental verification on the BRUKER 750 MHz NMR spectrometer of the composite pulses are also presented in this paper.

1. Introduction

Broadband excitation for wide chemical shift nuclei like ^{19}F, where the chemical shift can range over 600 ppm, is problematic as NMR signal intensity degrades towards the edges of full spectral width due to the resonance offset effect. Such nuclei require excitation of different spectra regions, at a field of 1 GHz, the target bandwidth is 50 kHz for excitation of entire 200 ppm ^{13}C chemical shifts. Because of the limited power availability of radiofrequency in pulsed excitation, signal intensity and phases distort for resonance offset effect and degrade the accuracy of signal integration. Research has been done to establish different pulse techniques for broadband excitation and inversion over time to reduce the phase variation as a function of resonance offset. Some of these methods are optimal control techniques for pulse design [1–5], Rotating frame approximation method [6], adiabatic pulses [7–11], Polychromatic pulse technique [12], composite adiabatic pulses [13–17] etc. The method of composite pulses inevitably proves their efficacy in controlling the problems, as mentioned earlier. Research on producing various conventional composite pulses has developed [18–24]. Composite pulses are the sequence of closely spaced RF pulses, efficient to excite and invert the bulk magnetization over the broad spectral range and refocus the magnetization to eliminate the phase distortion as a function of the offset resonance frequency. Composite pulses, which are the sequence of ordered chirped-pulse for the application on ultra-broadband resonance frequency range, i.e., **CHORUS** are less sensitive to the degradation of the signal intensity over the full spectral range [25,26].

The main focus of this paper is an analytical explanation of the composite pulse **CHORUS** for broadband excitation, where the chirp pulses of different sweep rates are applied for excitation and refocussing of the magnetization. In [27] an analytical explanation for the forward sweep **CHORUS** sequence for chirp excitation is provided. Whereas this paper emphasizes the reverse sweep **CHORUS** sequence and the combination of both. Other analytical explanations are also present for broadband excitation and inversion using the chirp mechanism in [28,29], but this paper explains it differently. The composite adiabatic pulse sequence, **CHORUS**, is based on the phase modulation scheme, which has a chirp excitation pulse component that rotates the bulk magnetization to the equator from the north pole. The chirp excitation pulse produces a three-stage rotation to bring the magnetization to the equator, but it has some non-uniform phases, depending on the resonance offset. The inversion chirp pulse with the double sweep rate can remove the phase dispersion and refocus the non-uniform

Abbreviations: CHORUS, CHirped ORdered Ultrabroadband Spectroscopy.

* Corresponding author.
E-mail addresses: sreya@sc.iitb.ac.in, sreya_das@iitb.ac.in (S. Das).

https://doi.org/10.1016/j.jmr.2022.107359
1090-7807/

phase. The inversion pulse is purely adiabatic and follows the adiabaticity condition $\dot{\theta} \ll \omega_{eff}$, which indicates that the rate of change of the direction of the effective magnetic field is much slower than the precession frequency of the magnetizing vector around the effective magnetic field. We have achieved the condition, $a \ll A^2$ from the adiabatic condition of the chirp pulse, where a is the sweep rate or chirp rate and A is the amplitude of the pulse. However, rotation due to the excitation pulse can be explained as three stage rotation, where the first and third stages are adiabatic but not the second stage. The chirp rate of the excitation pulse is kept very high $a > A^2$, and for this paper $a = 2.77A^2$. One inversion pulse after the excitation pulse is not fully efficient in removing the phase dispersion, and hence a second inversion pulse is applied to minimize the uniform phase [27]. The combination of these three chirp pulses is the **CHORUS** pulse sequence and is used to excite the arbitrarily large bandwidth without increasing the peak amplitude of the pulse. In this paper, the chirp pulses are classified depending on the forward and reverse sweep rate, where both forward and reverse chirp pulses can do excitation and inversion of the magnetization. There are four possible cases of chirp excitation. In the first case, all the excitation and refocussing pulses have a forward sweep, and in the second case, all the pulses change to a reverse sweep rate. The ratio of the amplitudes of the second refocusing pulse to the third refocusing pulse is $\frac{1}{\sqrt{2}}$ for these two cases to achieve the minimum phase dispersion. The third and fourth cases combine the forward and reverse chirp pulses for excitation and refocussing of the magnetization. In these cases, the ratio of the amplitudes of the second pulse to the third pulse is $\sqrt{2}$. Phase dispersion for all the above cases is obtained analytically, which exhibits a preferable performance of broadband excitation. Experimental and simulation results are provided with the simulated pulse to the **BRUKER** 750 MHz NMR spectrometer to obtain the NMR spectrum for the mixture of 99.5% D_2O and 0.5% H_2O.

2. Theory

The Bloch equation of the magnetizing vector for resonance offset $\Delta\omega$ of chemical shift is

$$\dot{X} = (\Delta\omega\Omega_z + A\cos\phi\Omega_x + A\sin\phi\Omega_y)X, \tag{1}$$

where,

$$\Omega_x = \begin{bmatrix} 0 & 0 & 0 \\ 0 & 0 & -1 \\ 0 & 1 & 0 \end{bmatrix}, \ \Omega_y = \begin{bmatrix} 0 & 0 & 1 \\ 0 & 0 & 0 \\ -1 & 0 & 0 \end{bmatrix}, \ \Omega_z = \begin{bmatrix} 0 & -1 & 0 \\ 1 & 0 & 0 \\ 0 & 0 & 0 \end{bmatrix},$$

are the generators of rotation and, A and ϕ are the strength and phase angle of the rf-field. Consider, $\exp(\theta\Omega_z)$ represents the rotation by θ flip angle around z– direction.

Chirp excitation pulse is explained as three stage rotation using forward sweep rate in [27]. The excitation is also possible using the negative sweep rate - reverse sweep excitation pulse. The following sections elaborate the excitation of the magnetizing vector using forward and reverse sweep mechanism.

2.1. Chirp Excitation - Forward sweep

The motivation of broadband control is to sweep the resonance frequency ω_0 over the range of $\Delta\omega$. The range of the offset frequency ω_0 is chosen within the range $[-B, B]$ and the sweep bandwidth is $[-C, C]$ with the sweep rate $a = \frac{2C}{T}$, where T is the sweep duration. Fig. 1 shows the trapezoidal forward sweep chirp pulse with the above-mentioned ranges.

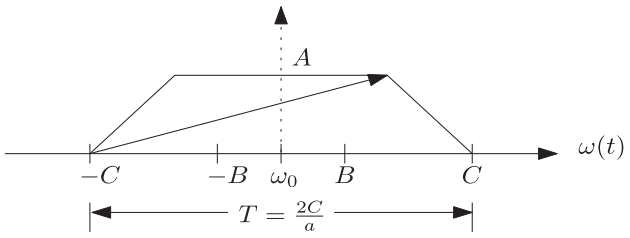

Fig. 1. Trapezoidal forward chirp pulse of strength A, sweep rate a, offset range $[-B, B]$ and sweep bandwidth $[-C, C]$.

2.1.1. Forward chirp pulse

In the forward sweep the phase $\phi(t)$ in (1) follows the trajectory

$$\dot{\phi}(t) = \omega(t) = -C + at,$$

hence,

$$\phi(t) = -Ct + \frac{1}{2}at^2.$$

2.1.2. Excitation mechanism

The chirp excitation pulse is represented by rotations in three stages, shown in Fig. 2, where the second stage does not follow the adiabaticity condition. Stage *I* rotation is in the off-resonance part of ω. It follows adiabaticity condition for time t_1 for the range of $\omega(t)$ is $[-C, \omega_0 - \beta A]$. It is represented as $\exp(\theta_0\Omega_y)$ and $\beta = \cot\theta_0$. Stage *II* rotation is near the offset for time t_2 and experience resonance within the range $[\omega_0 - \beta A, \omega_0 + \beta A]$ of $\omega(t)$. It doesnot follow adiabaticity condition and it is represented by the rotation $\exp(\alpha\Omega_x)$. Stage *III* rotation is again adiabatic rotation and in the off-resonance part sweeping within the range $[\omega_0 + \beta A, C]$ of $\omega(t)$. This rotation is represented as $\exp(\theta_0\Omega_y)$. Fig. 3 shows the evolution of the magnetization vector with the effective field in the three stages of the excitation pulse. The angle of rotations satisfy the condition $\cos\alpha = \tan^2\theta_0$ for excitation. Time taken for the stage *III* rotation is t_3 and the total time taken for the excitation pulse is T. From the Bloch Eq. (1), changing the co-ordinate to the reference frame of $\phi(t)$ by considering the new co-ordinate $Y = \exp(-\phi(t)\Omega_z)X$, we obtain

$$\dot{Y} = \omega_{eff}[\cos(\theta(t))\Omega_z + \sin(\theta(t))\Omega_x]Y, \tag{2}$$

where, $\omega_{eff} = \sqrt{(\omega_0 - \omega(t))^2 + A^2}$ and $\tan(\theta(t)) = \frac{A}{\omega_0 - \omega(t)}$. Again, changing the co-ordinate in the reference frame of $\theta(t)$ by taking $Z = \exp(-\theta(t)\Omega_y)Y$, the state equation is

$$\dot{Z}(t) = \left(-\dot{\theta}(t)\Omega_y + \omega_{eff}\Omega_z\right)Z(t). \tag{3}$$

For the adiabaticity condition, $\omega_{eff} \gg \dot{\theta}(t), \dot{\theta}(t)$ avarages out and the solution of (3) is

$$Z(T_f) = \exp\left(\int_0^{T_f} \omega_{eff}dt\Omega_z\right)Z(0), \tag{4}$$

where, T_f is the time taken for the rotation in each stage. Representing (4) in terms of the Y-coordinate, we get

$$Y(T_f) = \exp\left(\theta(T_f)\Omega_y\right)\exp\left(\int_0^{T_f} \omega_{eff}dt\Omega_z\right)\exp\left(-\theta(0)\Omega_y\right)Y(0). \tag{5}$$

The total time taken for first stage rotation is t_1. hence at the end of the stage *I* rotation, $T_f = t_1$, and the final state (5) is

$$Y(t_1) = \exp\left(\theta(t_1)\Omega_y\right)\exp\left(\int_0^{t_1} \omega_{eff}dt\Omega_z\right)\exp\left(-\theta(0)\Omega_y\right)Y(0). \tag{6}$$

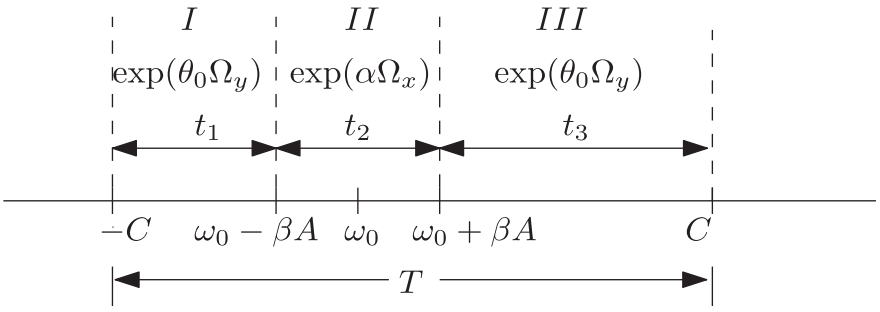

Fig. 2. Schematic diagram of three stage rotation of forward excitation chirp pulse.

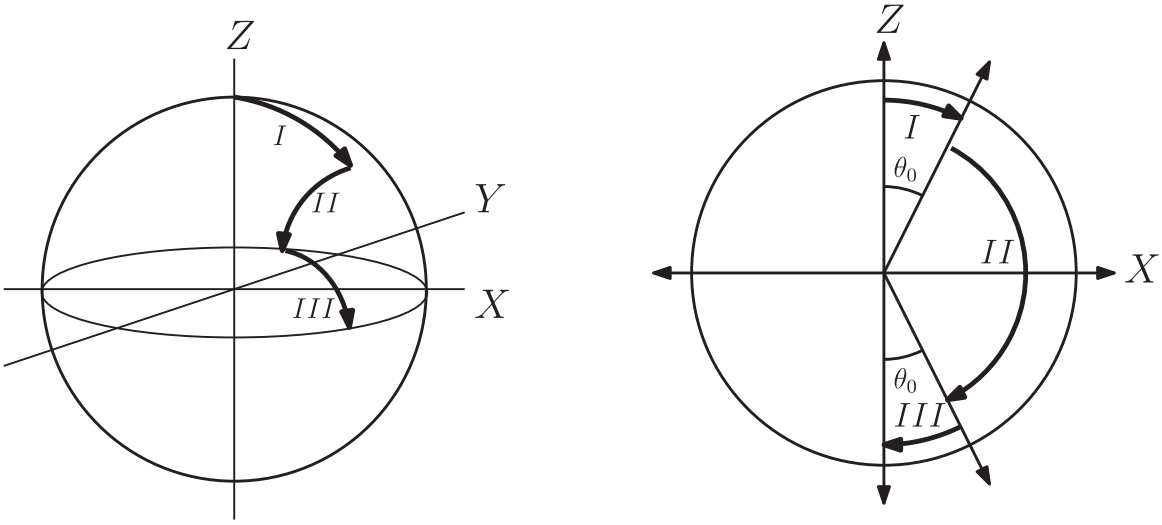

(a) The figure shows the evolution of the magnetizing vector in the reference frame of phase, $\phi(t)$. First stage rotation around $y-$axis, second stage around $z-$axis and third stage again around $y-$axis.

(b) The figure shows the angle of rotation of the effective field in the three stages of excitation pulse. In first stage effective field starts from $z-$axis and rotated by angle θ_0. In second stage the effective field is rotated by angle α and makes an angle θ_0 with $-z$ axis and in the final stage it ends up at the $-z$ axis.

Fig. 3. Evolution of the magnetization vector with the effective field in the three stages of the excitation pulse.

For excitation with forward sweep the entire rotation of the Bloch vector around y–axis is $\theta(t) = 0$ to $\theta(t) = \pi$. For the first stage rotation, let, $\cot\theta_0 = \beta$, where, the flip angle is θ_0. Therefore, at $t = 0, \theta(0) = 0$, and at the end of the first stage, $\theta(t_1) = \theta_0$. So, (6) reduced to

$$Y(t_1) = \exp\left(\theta_0\Omega_y\right)\exp\left(\int_0^{t_1}\omega_{eff}dt\Omega_z\right)Y(0). \tag{7}$$

The term $\exp\left(\int_0^{t_1}\omega_{eff}dt\Omega_z\right)$ in (7) denotes the rotation around z–axis and $Y(0)$ is also the vector along z–axis, so the term $\exp\left(\int_0^{t_1}\omega_{eff}dt\Omega_z\right)Y(0)$ gives the $Y(0)$ itself. Now, $Y(0) = \exp(-\phi(0)\Omega_z)X(0) = X(0)$ as $\phi(0) = 0$. Therefore, $Y(0) = X(0) = \begin{bmatrix}0\\0\\1\end{bmatrix}$. Hence,

$$Y(t_1) = \exp(\theta_0\Omega_y)Y(0) = \begin{bmatrix}\sin\theta_0\\0\\\cos\theta_0\end{bmatrix}. \tag{8}$$

Second stage rotation is non-adiabatic that implies the condition $\omega_{eff} \gg \dot{\theta}(t)$ is not followed. Let consider the sweep rate, $a = \beta^2A^2$, for $\beta > 1$. The range of $\omega(t)$ in stage II is $[\omega_0 - \beta A, \omega_0 + \beta A]$, therefore the time taken for the second stage rotation $t_2 = \frac{2\beta A}{a} = \frac{2}{\beta A}$. Let in the second stage, the angle of rotation is α, then $\alpha = At_2 = \frac{2}{\beta}$, therefore, $t_2 = \frac{\alpha}{A}$. The rotation in this stage is non-adiabatic, so, considering the Bloch equation before averaging out $\dot{\theta}$, hence the equation of motion in the second stage, from (2) is

$$\dot{Y} = [(\omega_0 - \omega(t))\Omega_z + A\Omega_x]Y. \tag{9}$$

The solution of (9) is

$$Y(t) = \exp\left(\int_0^{\frac{\alpha}{A}}[(\omega_0 - \omega(t))\Omega_z + A\Omega_x]dt\right)Y(0).$$

The term, $\exp\left(\int_0^{\frac{\alpha}{A}}[(\omega_0 - \omega(t))\Omega_z + A\Omega_x]dt\right)$ gives α angle rotation around x–axis therefore it is written as $\exp(\alpha\Omega_x)$, hence, substituting $Y(t_1)$ from (8), at the end of the second stage rotation the magnetizing vector is

$$Y(t_2) = \exp(\alpha\Omega_x)Y(t_1) = \begin{bmatrix} \sin\theta_0 \\ -\sin\alpha\cos\theta_0 \\ \cos\alpha\cos\theta_0 \end{bmatrix}. \quad (10)$$

Third stage rotation is again adiabatic for the range of $\omega(t)$ in $[\omega_0 + \beta A, C]$, for the time instant t_3 and angle of rotation in the time instant in θ_0. Considering only the time period for third stage the final state can be written from (5). In the third stage the rest of the angle around y–axis is rotated to make the z–coordinate 0, so, $\theta(0) = \pi - \theta_0$ and $\theta(t_3) = \pi$. Hence the final state from (5) is,

$$Y(T) = \exp(\pi\Omega_y)\exp\left(\int_0^{t_3}\omega_{eff}dt\Omega_z\right)\exp((\theta_0 - \pi)\Omega_y)Y(0).$$

Using Baker-Campbell-Hausdorff formula $Y(T)$ further reduced to,

$$Y(T) = \exp\left(-\int_0^{t_3}\omega_{eff}dt\Omega_z\right)\exp(\theta_0\Omega_y)Y(0). \quad (11)$$

Substituting (10) to (11), the final state after the third stage is,

$$Y(T) = \exp\left(-\int_0^{t_3}\omega_{eff}dt\Omega_z\right)\exp(\theta_0\Omega_y)\begin{bmatrix} \sin\theta_0 \\ -\sin\alpha\cos\theta_0 \\ \cos\alpha\cos\theta_0 \end{bmatrix}. \quad (12)$$

The last term of (12),

$$\exp(\theta_0\Omega_y)\begin{bmatrix} \sin\theta_0 \\ -\sin\alpha\cos\theta_0 \\ \cos\alpha\cos\theta_0 \end{bmatrix} = \begin{bmatrix} \sin\theta_0\cos\theta_0(1+\cos\alpha) \\ -\sin\alpha\cos\theta_0 \\ -\sin^2\theta_0 + \cos^2\theta_0\cos\alpha \end{bmatrix}. \quad (13)$$

The vector to be in equator, the last term of (13), $-\sin^2\theta_0 + \cos^2\theta_0\cos\alpha = 0$ which gives, $\tan^2\theta_0 = \cos\alpha$, which is the chirp excitation condition. The chirp excitation condition implies, $\frac{1}{\beta^2} = \cos\left(\frac{2}{\beta}\right)$, which gives the solution $\beta^2 = 2.81$. Hence, the sweep rate $a = \beta^2A^2 = 2.81A^2$ for the chirp excitation pulse. For simulation and experiment we have considered the sweep rate $a = 2.77A^2$. The term,

$$\int_0^{t_3}\omega_{eff}(t)dt = \frac{1}{a}\int_{\omega_0+\beta A}^{C}\omega_{eff}(\omega)d\omega = \Phi(\omega_0), \quad (14)$$

introduces a rotation $\exp(\Phi(\omega_0)\Omega_z)$ of phase factor $\Phi(\omega_0)$, which de-phases the Bloch vector in $x - y$ plane.

2.2. Chirp Excitation - Reverse sweep

For the reverse sweep case, the range of the offset frequency ω_0 is chosen within the range $[B, -B]$ and the sweep bandwidth is $[C, -C]$ with sweep rate $a = \frac{2C}{T}$, where, T is the sweep duration. The Fig. 4 shows the trapezoidal chirp pulse for the reverse sweep with the above-mentioned ranges.

2.2.1. Reverse chirp pulse

In the reverse sweep the phase $\phi(t)$ in (1) follows the trajectory

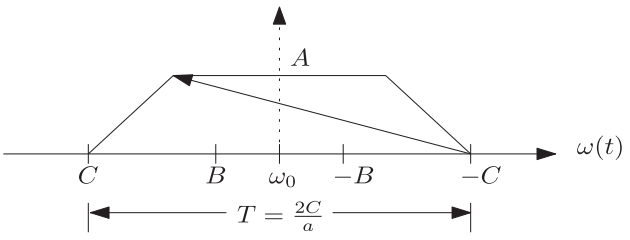

Fig. 4. Trapezoidal reverse chirp pulse of strength A, sweep rate a, offset range $[B, -B]$ and sweep bandwidth $[C, -C]$.

$$\dot{\phi}(t) = \omega(t) = C - at,$$

hence,

$$\phi(t) = Ct - \frac{1}{2}at^2.$$

2.2.2. Excitation mechanism

The reverse chirp excitation pulse is also represented as three stage rotations as similar as forward chirp excitation, shown in diagram in Fig. 5. Here, stage I rotation is in the range of $\omega(t)$ is $[C, \omega_0 + \beta A]$. Stage II rotation is within the range $[\omega_0 + \beta A, \omega_0 - \beta A]$ of $\omega(t)$. And, stage III rotation is within the range $[\omega_0 - \beta A, -C]$ of $\omega(t)$. The second stage is the non-adiabatic stage of the rotation. It also satisfies the chirp condition $\cos\alpha = \tan^2\theta_0$. For reverse sweep pulse the angle of rotation around y–axis is from $\theta(t) = \pi$ to $\theta(t) = 0$. The Bloch vector in the $\phi(t)$ rotating frame at the end of the first stage is written from (5), where at $t = 0, \theta(0) = \pi$, as the rotation is negative. At time t_1 let it rotated by angle θ_0,, therefore, $\theta(t_1) = \theta(T) = \pi - \theta_0$, hence

$$Y(t_1) = \exp((\pi - \theta_0)\Omega_y)\exp\left(\int_0^{t_1}\omega_{eff}dt\Omega_z\right)\exp(-\pi\Omega_y)Y(0). \quad (15)$$

Simplifying $Y(t_1)$ in (15) with Baker-Campbell-Hausdorff formula and substituting $Y(0)$ for $\phi(0) = 0$ obtains as

$$Y(t_1) = \exp(-\theta_0\Omega_y)\exp\left(-\int_0^{t_1}\omega_{eff}dt\Omega_z\right)Y(0) = \exp(-\theta_0\Omega_y)Y(0) = \begin{bmatrix} -\sin\theta_0 \\ 0 \\ \cos\theta_0 \end{bmatrix}. \quad (16)$$

Similarly, using (16), at the end of the second stage rotation the magnetizing vector is

$$Y(t_2) = \exp(\alpha\Omega_x)Y(t_1) = \begin{bmatrix} -\sin\theta_0 \\ -\sin\alpha\cos\theta_0 \\ \cos\alpha\cos\theta_0 \end{bmatrix}. \quad (17)$$

Third stage rotation is again adiabatic for the range of $\omega(t)$ in $[\omega_0 - \beta A_1, -C]$, and at the end of total time is T in Fig. 5, the final state of the Bloch vector is written as (5) and the rest of the angle around y–axis is rotated to make the y–coordinate 0, so, $\theta(0) = \theta_0$ and $\theta(T) = 0$. The final state is hence,

$$Y(T) = \exp\left(\int_0^{t_3}\omega_{eff}dt\Omega_z\right)\exp(-\theta(0)\Omega_y)\begin{bmatrix} -\sin\theta_0 \\ -\sin\alpha\cos\theta_0 \\ \cos\alpha\cos\theta_0 \end{bmatrix}. \quad (18)$$

The term in (18),

$$\exp(-\theta(0)\Omega_y)\begin{bmatrix} -\sin\theta_0 \\ -\sin\alpha\cos\theta_0 \\ \cos\alpha\cos\theta_0 \end{bmatrix} = \begin{bmatrix} -\sin\theta_0\cos\theta_0(1+\cos\alpha) \\ -\sin\alpha\cos\theta_0 \\ -\sin^2\theta_0 + \cos^2\theta_0\cos\alpha \end{bmatrix}. \quad (19)$$

The vector to be in equator, the last term of (19), $-\sin^2\theta_0 + \cos^2\theta_0\cos\alpha = 0$ which gives, $\tan^2\theta_0 = \cos\alpha$, the chirp excitation condition, which gives $\beta^2 = 2.81$ and the sweep rate $a = \beta^2A^2 = 2.81A^2$. We have considered sweep rate $a = 2.77A^2$ for simulation and experiment. The dephasing factor for this case is

$$\Phi(\omega_0) = \int_0^{t_3}\omega_{eff}(t)dt = -\frac{1}{a}\int_{\omega_0-\beta A}^{-C}\omega_{eff}(\omega)d\omega, \quad (20)$$

which introduces a rotation $\exp(\Phi(\omega_0)\Omega_z)$ and de-phases the Bloch vector in $x - y$ plane.

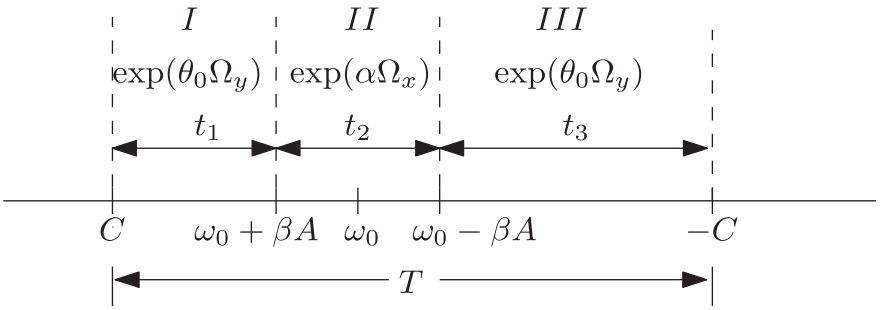

Fig. 5. Schematic diagram of three stage rotation of reverse excitation pulse.

2.3. Chirp inversion

The inversion pulse is adiabatic pulse and follows the adiabaticity condition, $\omega_{eff} \gg \dot{\theta}(t)$, which leads to $a \ll A^2$ where, $\dot{\theta}(t) = \frac{Aa}{\omega_{eff}^2}$, for forward sweep. The positive $\dot{\theta}$ implies $\theta(t)$ is increasing starting from $\theta(0) = 0$ to $\theta(T) = \pi$. Let us recall the final state of the Bloch vector in the $\phi(t)$ reference frame from (5) and for the boundary condition of $\theta(t), \theta(T) = \pi$ and $\theta(0) = 0$, hence, (5) reduced to,

$$Y(T) = \exp(\pi\Omega_y) \exp\left(\int_0^T \omega_{eff} dt \Omega_z\right) Y(0). \tag{21}$$

And, as $\phi(T) = 0 = \phi(0)$, for $t = T = \frac{2C}{a}$, the Bloch vector from (21) is

$$X(T) = \exp(\pi\Omega_y) \exp\left(\int_0^T \omega_{eff} dt \Omega_z\right) X(0). \tag{22}$$

Hence, from (22) the propagator for forward inversion pulse is,

$$\exp(\pi\Omega_y) \exp\left(\int_0^T \omega_{eff} dt \Omega_z\right). \tag{23}$$

For the reverse sweep inversion pulse, to follow the adiabaticity condition, $\omega_{eff} \gg \dot{\theta}(t)$, we consider $a \ll A^2$, where, $\dot{\theta}(t) = -\frac{Aa}{\omega_{eff}^2}$. The negative $\dot{\theta}$ implies $\theta(t)$ is decreasing starting from $\theta(0) = \pi$ to $\theta(T) = 0$. Again, recalling the final state of the Bloch vector in the $\phi(t)$ reference frame from (5) and for the boundary condition of $\theta(t), \theta(T) = 0$ and $\theta(0) = \pi$, (5) reduced to,

$$Y(T) = \exp\left(\int_0^T \omega_{eff} dt \Omega_z\right) \exp(-\pi\Omega_y) Y(0). \tag{24}$$

And, as $\phi(T) = 0 = \phi(0)$, for $t = T = \frac{2C}{a}$ the Bloch vector from (24) is

$$X(T) = \exp\left(\int_0^T \omega_{eff} dt \Omega_z\right) \exp(-\pi\Omega_y) X(0). \tag{25}$$

Hence, from (25) the propagator for reverse inversion pulse is

$$\exp\left(\int_0^T \omega_{eff} dt \Omega_z\right) \exp(-\pi\Omega_y). \tag{26}$$

2.4. Composite pulses for broadband excitation

The de-phasing factor due the single excitation pulse, is removed with double refocussing mechanism. The three pulse sequence, one excitation pulse and two refocussing pulses, form a composite pulse. The detailed analytical explanation of this double refocussing is provided in [27]. The following section explains the feasible combinations of forward and reverse chirp pulses to form the composite pulse sequence, which refocusses the Bloch vector.

2.4.1. F-F-F pulse

In F-F-F pulse sequence the forward excitation pulse is followed by two forward inversion pulses for the time period T, T and $\frac{T}{2}$ respectively and the amplitude of the last inversion pulse is $\sqrt{2}$ times of the second inversion pulse. A free-evolution for time-period $\frac{T}{2}$ is added before the last pulse. The diagram is shown in Fig. 6. The propagators of the refocussing pulses from (23) are written as

$$\exp(\pi\Omega_y) \exp\left(\int_0^{\frac{T}{2}} \omega''_{eff}(t) dt \Omega_z\right) \exp\left(\frac{\omega_0 T}{2}\Omega_z\right) \exp(\pi\Omega_y) \exp\left(\int_0^T \omega\prime_{eff}(t) dt \Omega_z\right), \tag{27}$$

where, ω'_{eff} and ω''_{eff} are the phase dispersion for the first and second refocussing pulse respectively. Reducing (27) using Baker-Campbell-Hausdorff, we get,

$$\exp\left(-\int_0^{\frac{T}{2}} \omega''_{eff}(t) dt \Omega_z\right) \exp\left(-\frac{\omega_0 T}{2}\Omega_z\right) \exp\left(\int_0^T \omega'_{eff}(t) dt \Omega_z\right). \tag{28}$$

Therefore the phase dispersion from (28) and (14) as the function of offset frequency is

$$\Phi(\omega_0) = -\frac{1}{2a}\int_{-C}^{C} \omega''_{eff}(\omega) d\omega + \frac{1}{a}\int_{-C}^{C} \omega'_{eff}(\omega) d\omega - \frac{1}{a} \times \int_{\omega_0+\beta A_1}^{C} \omega_{eff}(\omega) d\omega. \tag{29}$$

The last term in (29) is due to the third stage of the excitation $\frac{\pi}{2}$ pulse. Let, the amplitudes of the excitation $\frac{\pi}{2}$ pulse and two inversion π pulse are A_1, A_2 and A_3 respectively, where, $A_3 = \sqrt{2}A_2$. Considering, $\omega_{eff}(\omega) = \sqrt{(\omega_0-\omega)^2 + A_1^2} = (\omega_0 - \omega) + \frac{1}{2}\frac{A_1^2}{(\omega_0-\omega)}$ for $(\omega_0 - \omega) > A_1$, $\omega'_{eff}(\omega) = \sqrt{(\omega_0-\omega)^2 + A_2^2} = (\omega_0 - \omega) + \frac{1}{4}\frac{A_3^2}{(\omega_0-\omega)}$ for $(\omega_0 - \omega) > A_2$, and $\omega''_{eff}(\omega) = \sqrt{(\omega_0-\omega)^2 + A_3^2} = (\omega_0 - \omega) + \frac{1}{2}\frac{A_3^2}{(\omega_0-\omega)}$ for $(\omega_0 - \omega) > A_3$, where, A_1 is the amplitude of the excitation pulse, A_2 and A_3 are the amplitude of the first and second refocussing pulse respectively.

Expanding $\Phi(\omega_0)$ in the resonance and off-resonance part of the sweeping frequency, the first term is

$$-\frac{1}{2a}\left[\int_{-C}^{\omega_0-A_3}\left((\omega_0-\omega) + \frac{1}{2}\frac{A_3^2}{(\omega_0-\omega)}\right)d\omega + \int_{\omega_0-A_3}^{\omega_0+A_3} \omega''_{eff}(\omega) d\omega + \int_{\omega_0+A_3}^{C}\left((\omega-\omega_0) + \frac{1}{2}\frac{A_3^2}{(\omega-\omega_0)}\right)d\omega\right]. \tag{30}$$

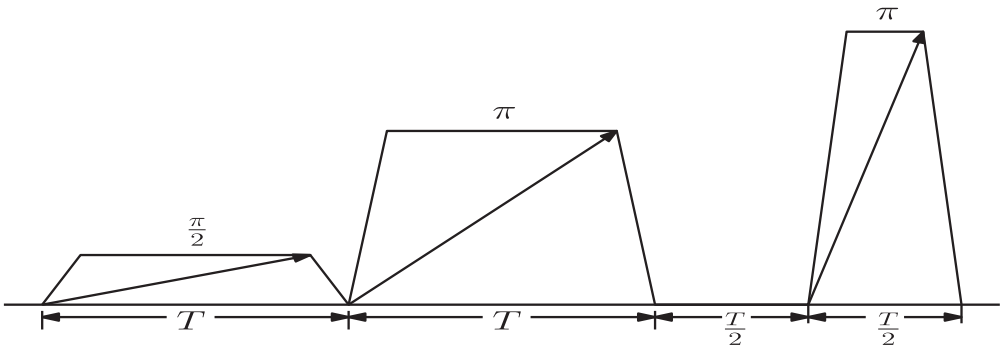

Fig. 6. Double refocussing F-F-F pulse; sequence of the chirp pulses are forward sweep excitation $\frac{\pi}{2}$ pulse of time-period T, forward sweep inversion π pulse of the same time-period, a free-evolution for time period $\frac{T}{2}$ and lastly a forward sweep inversion π pulse for time-period $\frac{T}{2}$. The amplitude of the last inversion pulse is $\sqrt{2}$ times of the first inversion pulse.

The second term of $\Phi(\omega_0)$ is

$$\frac{1}{a}\left[\int_{-C}^{\omega_0-A_3}\left((\omega_0-\omega)+\frac{1}{4}\frac{A_3^2}{(\omega_0-\omega)}\right)d\omega+\int_{\omega_0-A_3}^{\omega_0+A_3}\omega'_{eff}(\omega)d\omega+\int_{\omega_0+A_3}^{C}\left((\omega-\omega_0)+\frac{1}{4}\frac{A_3^2}{(\omega-\omega_0)}\right)d\omega\right], \tag{31}$$

and the third term is

$$-\frac{1}{a}\left[\int_{\omega_0+\beta A_1}^{\omega_0+A_3}\omega_{eff}(\omega)d\omega+\int_{\omega_0+A_3}^{C}\left((\omega-\omega_0)+\frac{1}{2}\frac{A_1^2}{(\omega-\omega_0)}\right)d\omega\right]. \tag{32}$$

The terms $\int_{\omega_0+A_3}^{\omega_0-A_3}\omega''_{eff}(\omega)d\omega$, $\int_{\omega_0+A_3}^{\omega_0-A_3}\omega'_{eff}(\omega)d\omega$ and $\int_{\omega_0-\beta A_1}^{\omega_0-A_3}\omega_{eff}(\omega)d\omega$, from (30), (31) and (32) respectively, are omitted as it does not show any non-uniform phase dispersion. From the rest of the terms considering all the linear terms for $(\omega_0-\omega)$ and adding $\frac{1}{2a}\int_{\omega_0-A_3}^{\omega_0+A_3}(\omega_0-\omega)d\omega$ as it contributes nothing to the expression, the linear terms of $\Phi(\omega_0)$ reduced to,

$$\frac{1}{2a}\int_{-C}^{\omega_0-A_3}(\omega_0-\omega)d\omega+\frac{1}{2a}\int_{\omega_0-A_3}^{\omega_0+A_3}(\omega_0-\omega)d\omega+\frac{1}{2a}\int_{\omega_0+A_3}^{C}(\omega_0-\omega)d\omega=\frac{1}{2a}\int_{-C}^{C}(\omega_0-\omega)d\omega. \tag{33}$$

The integration in (33) results in $\frac{\omega_0 T}{2}$, which indicates a free-evolution for time period $\frac{T}{2}$. Hence, the introduced free-evolution compensates the phase dispersion due to the linear terms of the refocussing pulses. The non-linear terms from (30) and (31) cancels each other effect and the remaining term is

$$-\frac{1}{2a}\int_{\omega_0+A_3}^{C}\frac{A_1^2}{(\omega-\omega_0)}d\omega. \tag{34}$$

The integration (34) provides the value of the phase dispersion as the function of the offset frequency,

$$\Phi(\omega_0)=\frac{A_1^2}{2a}\ln\left(\frac{A_3}{C-\omega_0}\right). \tag{35}$$

The maximum phase dispersion from (35) due to $\omega_0=B$ to $\omega_0=-B$ is

$$\Phi_{max}=\frac{A_1^2}{2a}\ln\left(\frac{1+B/C}{1-B/C}\right).$$

2.4.2. R-R-R pulse

In R-R-R pulse sequence the reverse excitation pulse is followed by two reverse inversion pulses for the time period T, T and $\frac{T}{2}$ respectively and the amplitude of the last inversion pulse is $\sqrt{2}$ times of the second inversion pulse. A free-evolution for time-period $\frac{T}{2}$ is added before the last pulse. The diagram is shown in Fig. 7. In this case the propagators of the refocussing pulses, from (26), are

$$\exp\left(\int_0^{\frac{T}{2}}\omega''_{eff}(t)dt\Omega_z\right)\exp\left(-\pi\Omega_y\right)\exp\left(\frac{\omega_0 T}{2}\Omega_z\right)\exp\left(\int_0^{T}\omega'_{eff}(t)dt\Omega_z\right)\exp\left(-\pi\Omega_y\right). \tag{36}$$

Simplifying (36) using Baker-Campbell-Hausdorff implies

$$\exp\left(\int_0^{\frac{T}{2}}\omega''_{eff}(t)dt\Omega_z\right)\exp\left(-\frac{\omega_0 T}{2}\Omega_z\right)\exp\left(-\int_0^{T}\omega'_{eff}(t)dt\Omega_z\right). \tag{37}$$

Therefore from (37) and (20) the phase dispersion is

$$\Phi(\omega_0)=-\frac{1}{2a}\int_{C}^{-C}\omega''_{eff}(\omega)d\omega+\frac{1}{a}\int_{C}^{-C}\omega'_{eff}(\omega)d\omega-\frac{1}{a}\int_{\omega_0-\beta A_1}^{-C}\omega_{eff}(\omega)d\omega. \tag{38}$$

The last term in (38) is due to the third stage of the excitation $\frac{\pi}{2}$ pulse. The amplitudes of the excitation $\frac{\pi}{2}$ pulse and two inversion π pulse are A_1, A_2 and A_3 respectively, where, $A_3=\sqrt{2}A_2$. Considering $\Phi(\omega_0)$ in (38) for the resonance and off-resonance offset frequency range, the first term is

$$-\frac{1}{2a}\left[\int_{C}^{\omega_0+A_3}\left((\omega-\omega_0)+\frac{1}{2}\frac{A_3^2}{(\omega-\omega_0)}\right)d\omega+\int_{\omega_0+A_3}^{\omega_0-A_3}\omega''_{eff}(\omega)d\omega+\int_{\omega_0-A_3}^{-C}\left((\omega_0-\omega)+\frac{1}{2}\frac{A_3^2}{(\omega_0-\omega)}\right)d\omega\right], \tag{39}$$

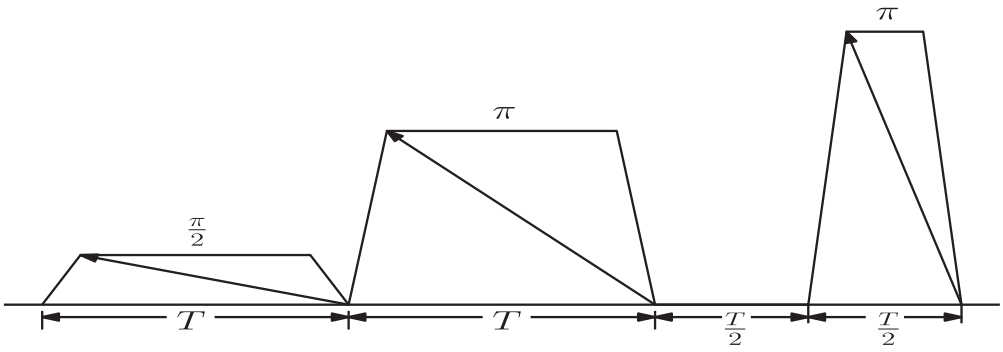

Fig. 7. Double refocussing R-R-R pulse; sequence of the chirp pulses are reverse sweep excitation $\frac{\pi}{2}$ pulse for time-period $\frac{T}{2}$, reverse sweep inversion π pulse of the same time-period, a free-evolution for time period $\frac{T}{2}$ and lastly a reverse sweep inversion π pulse for time-period $\frac{T}{2}$. The amplitude of the last inversion pulse is $\sqrt{2}$ times of the first inversion pulse.

the second term of $\Phi(\omega_0)$ is

$$\frac{1}{a}\left[\int_C^{\omega_0+A_3}\left((\omega-\omega_0)+\frac{1}{4}\frac{A_3^2}{(\omega-\omega_0)}\right)d\omega+\int_{\omega_0+A_3}^{\omega_0-A_3}\omega'_{eff}(\omega)da+\int_{\omega_0-A_3}^{-C}\left((\omega_0-\omega)+\frac{1}{4}\frac{A_3^2}{(\omega_0-\omega)}\right)d\omega\right], \tag{40}$$

and the third term is

$$-\frac{1}{a}\left[\int_{\omega_0-\beta A_1}^{\omega_0-A_3}\omega_{eff}(\omega)d\omega+\int_{\omega_0-A_3}^{-C}\left((\omega_0-\omega)+\frac{1}{2}\frac{A_1^2}{(\omega_0-\omega)}\right)d\omega\right]. \tag{41}$$

The terms $\int_{\omega_0+A_3}^{\omega_0-A_3}\omega''_{eff}(\omega)d\omega$, $\int_{\omega_0+A_3}^{\omega_0-A_3}\omega'_{eff}(\omega)d\omega$ and $\int_{\omega_0-\beta A_1}^{\omega_0-A_3}\omega_{eff}(\omega)d\omega$ from (39), (40) and (41) respectively, are omitted as it shows no dispersion with respect to ω_0. From the rest of the terms simplifying the linear terms in terms of $(\omega-\omega_0)$ and adding $\frac{1}{2a}\int_{\omega_0+A_3}^{\omega_0-A_3}(\omega-\omega_0)d\omega$ as it contributes nothing to the expression obtains the linear term as

$$\frac{1}{2a}\int_C^{\omega_0+A_3}(\omega-\omega_0)d\omega-\frac{1}{2a}\int_{\omega_0-A_3}^{-C}(\omega-\omega_0)d\omega+\frac{1}{2a}\int_{\omega_0+A_3}^{\omega_0-A_3}(\omega-\omega_0)d\omega=\frac{1}{2a}\int_C^{-C}(\omega-\omega_0)d\omega. \tag{42}$$

The integration in (42) gives $\frac{\omega_0 T}{2}$ which indicates a free-evolution for time period $\frac{T}{2}$. Hence, the introduced free-evolution compensates the phase dispersion due to the linear terms of the refocussing pulses. The non-linear terms in (39) and (40) cancels each other effect and the remaining term is

$$-\frac{1}{2a}\int_{\omega_0-A_3}^{-C}\frac{A_1^2}{(\omega_0-\omega)}d\omega. \tag{43}$$

Integration of (43) gives the phase dispersion as a function of offset frequency

$$\Phi(\omega_0)=\frac{A_1^2}{2a}\ln\left(\frac{\omega_0+C}{A_3}\right). \tag{44}$$

Hence, for this case the maximum phase dispersion from (44) due to $\omega_0=B$ to $\omega_0=-B$ is

$$\Phi_{max}=\frac{A_1^2}{2a}\ln\left(\frac{1+B/C}{1-B/C}\right).$$

2.4.3. F-R-R pulse

In F-R-R sequence a forward excitation pulse of time period T is followed by two reverse inversion pulses of time-period $\frac{T}{2}$ and T respectively and the amplitude of the first inversion pulse is $\sqrt{2}$ times of the second inversion pulse. The pulse sequence shown in Fig. 8 where a free-evolution of time-period $\frac{T}{2}$ is added before the last inversion pulse. Here, the propagators of the refocussing pulses from (26) are written as

$$\exp\left(\int_0^T\omega''_{eff}(t)dt\Omega_z\right)\exp\left(-\pi\Omega_y\right)\exp\left(\frac{\omega_0 T}{2}\Omega_z\right)\exp\left(\int_0^{\frac{T}{2}}\omega'_{eff}(t)dt\Omega_z\right)\exp\left(-\pi\Omega_y\right). \tag{45}$$

Using Baker-Campbell-Hausdorff to (45) reduces to

$$\exp\left(\int_0^T\omega''_{eff}(t)dt\Omega_z\right)\exp\left(-\frac{\omega_0 T}{2}\Omega_z\right)\exp\left(-\int_0^{\frac{T}{2}}\omega'_{eff}(t)dt\Omega_z\right). \tag{46}$$

Therefore, from (46), (14) and (20) the phase dispersion as a function of offset frequency is

$$\Phi(\omega_0)=-\frac{1}{a}\int_C^{-C}\omega''_{eff}(\omega)d\omega+\frac{1}{2a}\int_C^{-C}\omega'_{eff}(\omega)d\omega-\frac{1}{a}\int_{\omega_0+\beta A_1}^{C}\omega_{eff}(\omega)d\omega. \tag{47}$$

The last term in (47) is due to the third stage of the excitation $\frac{\pi}{2}$ pulse. As similar to above cases, the terms of $\Phi(\omega_0)$ are separated into resonance and off-resonance part and considering $A_2=\sqrt{2}A_3$, the first term is

$$-\frac{1}{a}\left[\int_C^{\omega_0+A_2}\left((\omega-\omega_0)+\frac{1}{4}\frac{A_2^2}{(\omega-\omega_0)}\right)d\omega+\int_{\omega_0+A_2}^{\omega_0-A_2}\omega''_{eff}(\omega)d\omega+\int_{\omega_0-A_2}^{-C}\left((\omega_0-\omega)+\frac{1}{4}\frac{A_2^2}{(\omega_0-\omega)}\right)d\omega\right]. \tag{48}$$

The second term of $\Phi(\omega_0)$ is

$$\frac{1}{2a}\left[\int_C^{\omega_0+A_2}\left((\omega-\omega_0)+\frac{1}{2}\frac{A_2^2}{(\omega-\omega_0)}\right)d\omega+\int_{\omega_0+A_2}^{\omega_0-A_2}\omega'_{eff}(\omega)d\omega+\int_{\omega_0-A_2}^{-C}\left((\omega_0-\omega)+\frac{1}{2}\frac{A_2^2}{(\omega_0-\omega)}\right)d\omega\right], \tag{49}$$

and the third term is

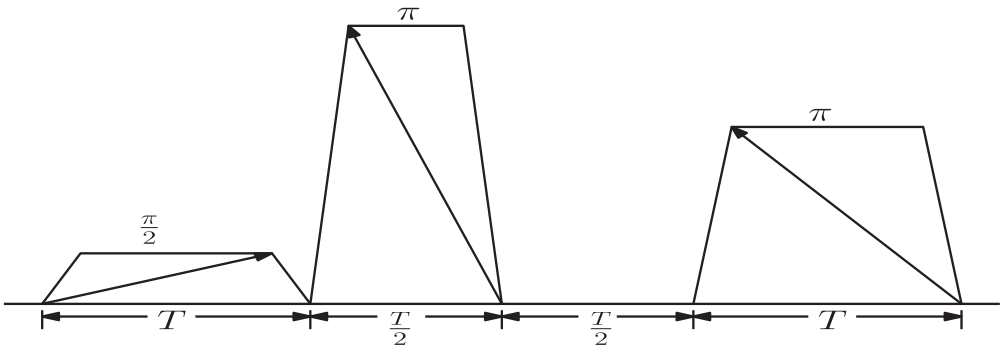

Fig. 8. Double refocussing F-R-R pulse; sequence of the chirp pulses are forward sweep excitation $\frac{\pi}{2}$ pulse for time-period T, reverse sweep inversion π pulse for time-period $\frac{T}{2}$, a free-evolution for time period $\frac{T}{2}$ and lastly a reverse sweep inversion π pulse for time-period T. The amplitude of the first inversion pulse is $\sqrt{2}$ times of the last inversion pulse.

$$-\frac{1}{a}\left[\int_{\omega_0+\beta A_1}^{\omega_0+A_2}\omega_{eff}(\omega)d\omega+\int_{\omega_0+A_2}^{C}\left((\omega-\omega_0)+\frac{1}{2}\frac{A_1^2}{(\omega-\omega_0)}\right)d\omega\right]. \tag{50}$$

First considering the linear terms $(\omega-\omega_0)$ from (48), (49) and (50) and omitting the terms which gives no dispersion, obtains

$$\frac{1}{2a}\int_{C}^{\omega_0+A_2}(\omega-\omega_0)d\omega+\frac{1}{2a}\int_{\omega_0-A_2}^{-C}(\omega-\omega_0)d\omega. \tag{51}$$

Adding $\frac{1}{2a}\int_{\omega_0+A_2}^{\omega_0-A_2}(\omega-\omega_0)d\omega$ to (51) as it contributes nothing to the expression obtains the linear term as

$$\frac{1}{2a}\int_{C}^{-C}(\omega-\omega_0)d\omega. \tag{52}$$

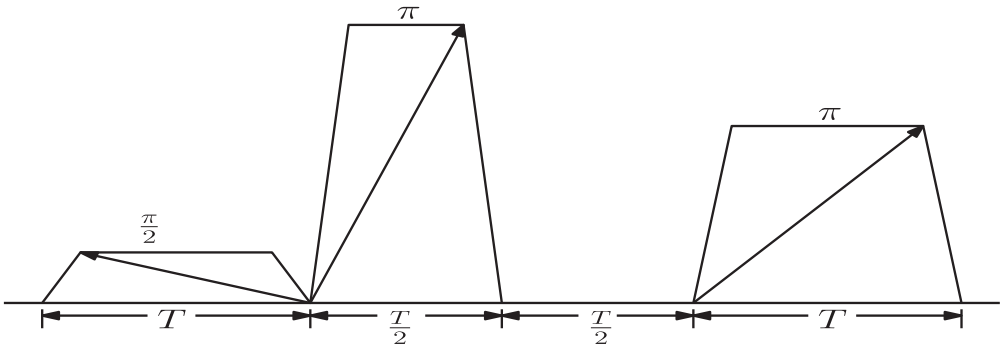

Fig. 9. Double refocussing R-F-F pulse; sequence of the chirp pulses are reverse sweep excitation $\frac{\pi}{2}$ pulse for time-period T, forward sweep inversion π pulse for time-period $\frac{T}{2}$, a free-evolution for time period $\frac{T}{2}$ and lastly a forward sweep inversion π pulse for time-period T. The amplitude of the first inversion pulse is $\sqrt{2}$ times of the last inversion pulse.

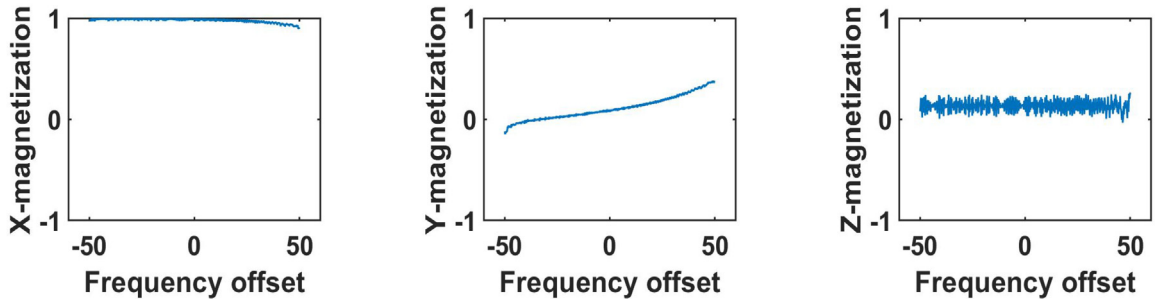

(a) X-magnetization vs frequency offset plot

(b) Y-magnetization vs frequency offset plot

(c) Z-magnetization vs frequency offset plot

Fig. 10. The final state of the magnetizing vector for F-F-F pulse, where the x–axis shows the frequency offset is varied over 100 *kHz* ($[-50, 50]$) range and the y–axis shows the X, Y and Z magnetization of the final state of the Bloch vector. The final state is $(1, 0, 0)$ in this case.

The integration in (52) results in $\frac{\omega_0 T}{2}$, which indicates a free-evolution for time period $\frac{T}{2}$ in the reverse chirp mechanism of refocussing. Hence, the introduced free-evolution compensates the phase dispersion due to the linear terms of the refocussing pulses. The non-linear terms from (48) and (49) cancels each other effect and the remaining term is

$$\frac{1}{2a}\int_{C}^{\omega_0+A_2}\frac{A_1^2}{(\omega_0-\omega)}d\omega, \tag{53}$$

and the result of (53) is the phase dispersion as the function of offset frequency

$$\Phi(\omega_0)=\frac{A_1^2}{2a}\ln\left(\frac{A_2}{C-\omega_0}\right). \tag{54}$$

Hence, the maximum phase dispersion of (54) due to $\omega_0 = B$ to $\omega_0 = -B$ is

$$\Phi_{max}=\frac{A_1^2}{2a}\ln\left(\frac{1-B/C}{1+B/C}\right).$$

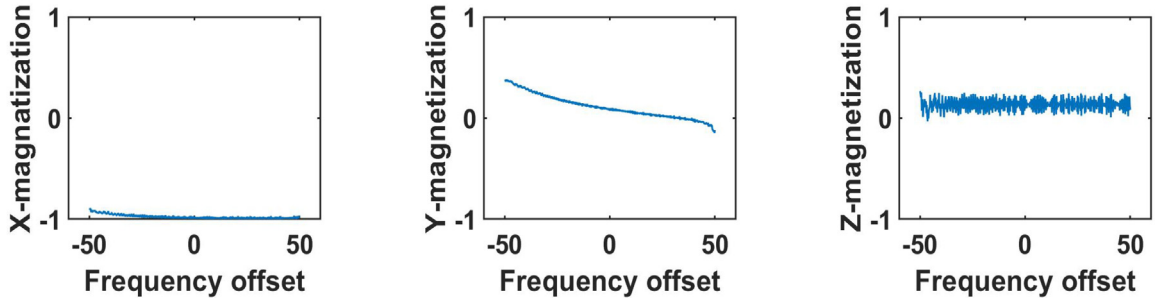

(a) X-magnetization vs frequency offset plot (b) Y-magnetization vs frequency offset plot (c) Z-magnetization vs frequency offset plot

Fig. 11. The final state of the magnetizing vector for R-R-R pulse, where the *x*–axis shows the frequency offset is varied over 100 *kHz* ($[-50, 50]$) range and the *y*–axis shows the X, Y and Z magnetization of the final state of the Bloch vector. The final state is $(-1, 0, 0)$ in this case.

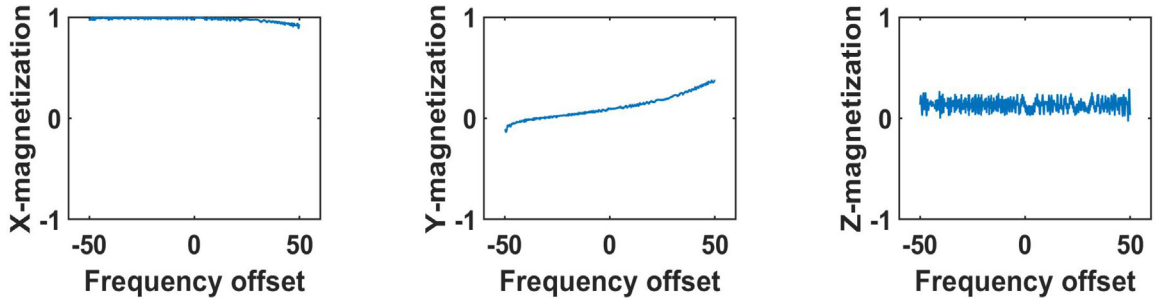

(a) X-magnetization vs frequency offset plot (b) Y-magnetization vs frequency offset plot (c) Z-magnetization vs frequency offset plot

Fig. 12. The final state of the magnetizing vector for F-R-R pulse, where the *x*–axis shows the frequency offset is varied over 100 *kHz* ($[-50, 50]$) range and the *y*– axis shows the X, Y and Z magnetization of the final state of the Bloch vector. The final state is $(1, 0, 0)$ in this case.

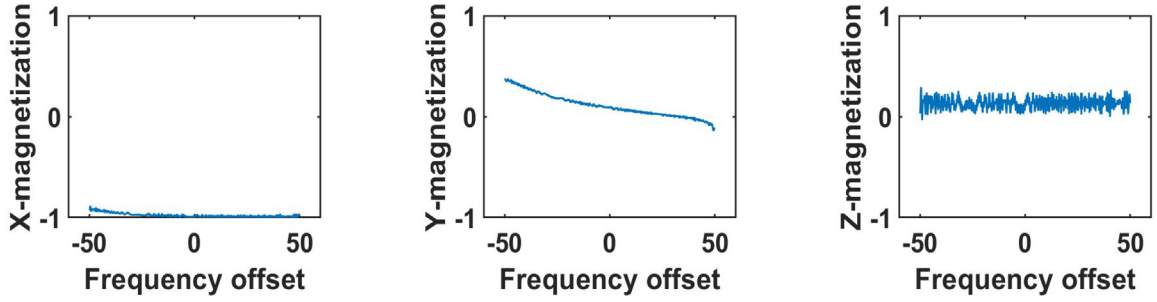

(a) X-magnetization vs frequency offset plot (b) Y-magnetization vs frequency offset plot (c) Z-magnetization vs frequency offset plot

Fig. 13. The final state of the magnetizing vector for R-F-F pulse, where the *x*– axis shows the frequency offset is varied over 100 *kHz* ($[-50, 50]$) range and the *y*– axis shows the X, Y and Z magnetization of the final state of the Bloch vector. The final state is $(-1, 0, 0)$ in this case.

2.4.4. R-F-F pulse

In R-F-F sequence a reverse excitation pulse of time period T is followed by two forward inversion pulses of time-period $\frac{T}{2}$ and T respectively and the amplitude of the first inversion pulse is $\sqrt{2}$ times of the second inversion pulse. The pulse sequence shown in Fig. 9 where a free-evolution of time-period $\frac{T}{2}$ is added before the last inversion pulse. Here, the propagators of the refocussing pulses from (23) are written as

$$\exp(\pi\Omega_y)\exp\left(\int_0^T \omega''_{eff}(t)dt\Omega_z\right)\exp\left(\frac{\omega_0 T}{2}\Omega_z\right)\exp(\pi\Omega_y)\exp\left(\int_0^{\frac{T}{2}} \omega'_{eff}(t)dt\Omega_z\right). \tag{55}$$

Using Baker-Campbell-Hausdorff to (55) reduces to

$$\exp\left(-\int_0^T \omega''_{eff}(t)dt\Omega_z\right)\exp\left(-\frac{\omega_0 T}{2}\Omega_z\right)\exp\left(\int_0^{\frac{T}{2}} \omega'_{eff}(t)dt\Omega_z\right). \tag{56}$$

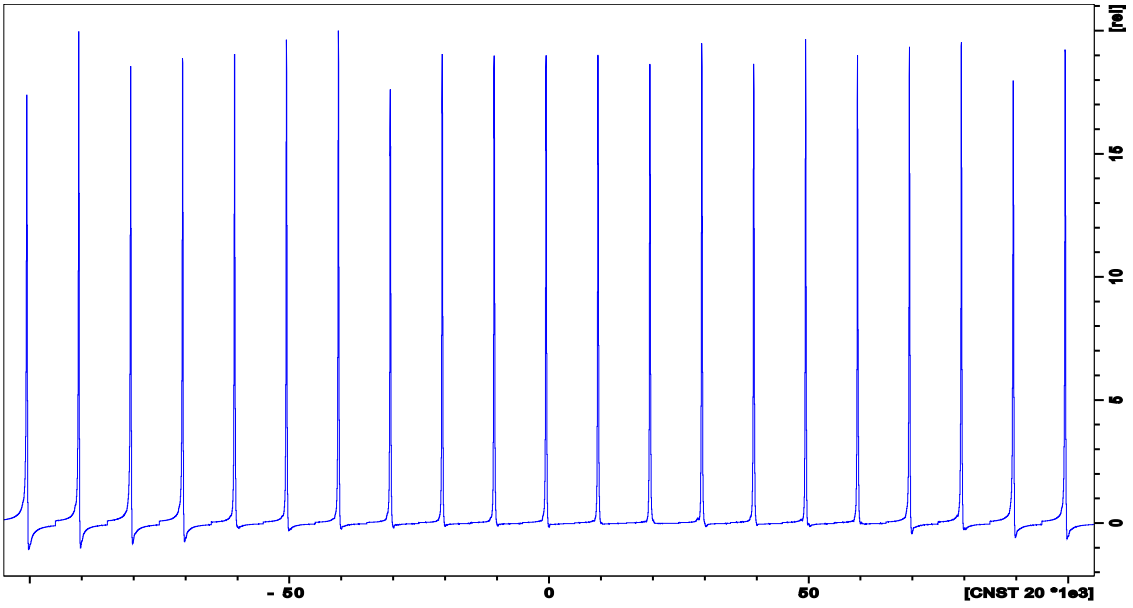

(a) Excitation profile for the simulated F-F-F pulse

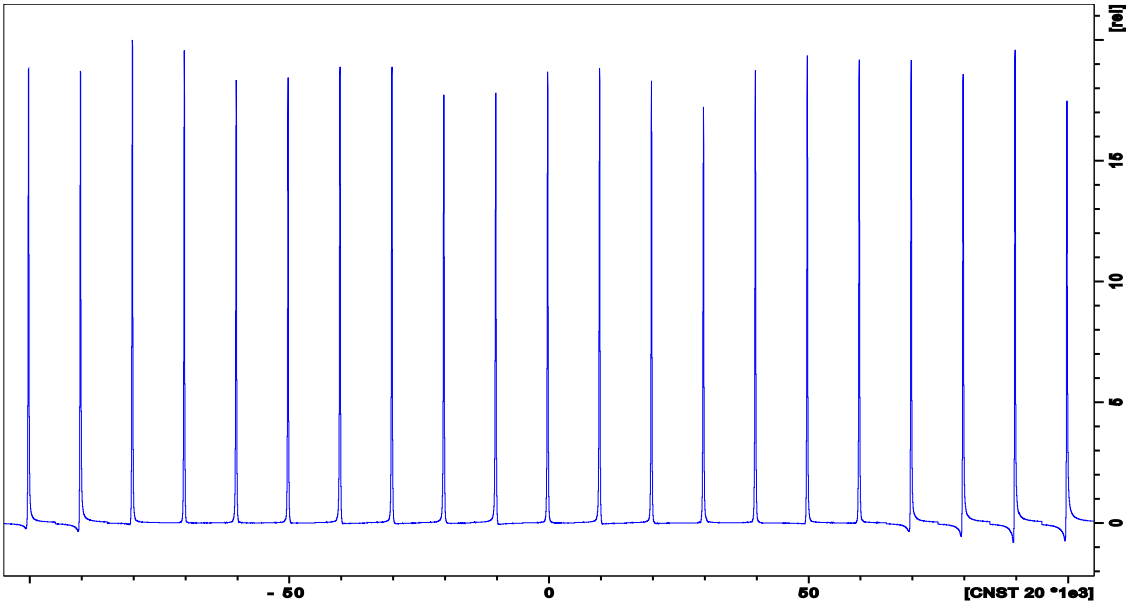

(b) Excitation profile for the simulated R-R-R pulse

Fig. 14. Excitation profiles of residual HDO signal in the mixture of 99.5% D_2O and 0.5% H_2O as sample for the F-F-F and R-R-R **CHORUS** pulses. The offset frequency is varied over the range 200 *kHz* ($[-100, 100]$) in the increment of 10 *kHz* along x– axis and the y– axis denotes the intensity of the spectrum.

Therefore, the phase dispersion from (56), (14) and (20) is written as

$$\Phi(\omega_0) = -\frac{1}{a}\int_{-C}^{C}\omega''_{eff}(\omega)d\omega + \frac{1}{2a}\int_{-C}^{C}\omega'_{eff}(\omega)d\omega - \frac{1}{a}\int_{\omega_0-\beta A_1}^{-C}\omega_{eff}(\omega)d\omega. \quad (57)$$

The last term in (57) is due to the third stage of the excitation $\frac{\pi}{2}$ pulse. The terms of $\Phi(\omega_0)$ are separated into resonance and off-resonance part and considering $A_2 = \sqrt{2}A_3$, the first term is

$$-\frac{1}{a}\left[\int_{-C}^{\omega_0-A_2}\left((\omega_0-\omega)+\frac{1}{4}\frac{A_2^2}{(\omega_0-\omega)}\right)d\omega + \int_{\omega_0-A_2}^{\omega_0+A_2}\omega''_{eff}(\omega)d\omega + \int_{\omega_0+A_2}^{C}\left((\omega-\omega_0)+\frac{1}{4}\frac{A_2^2}{(\omega-\omega_0)}\right)d\omega\right]. \quad (58)$$

The second term of $\Phi(\omega_0)$ is

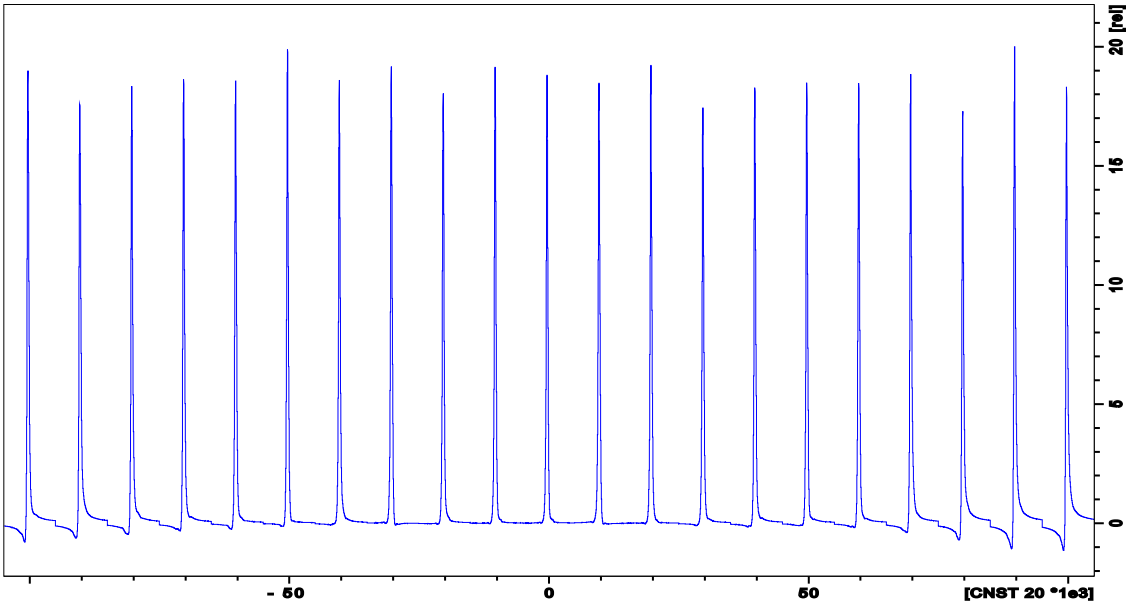

(a) Excitation profile for the simulated F-R-R pulse

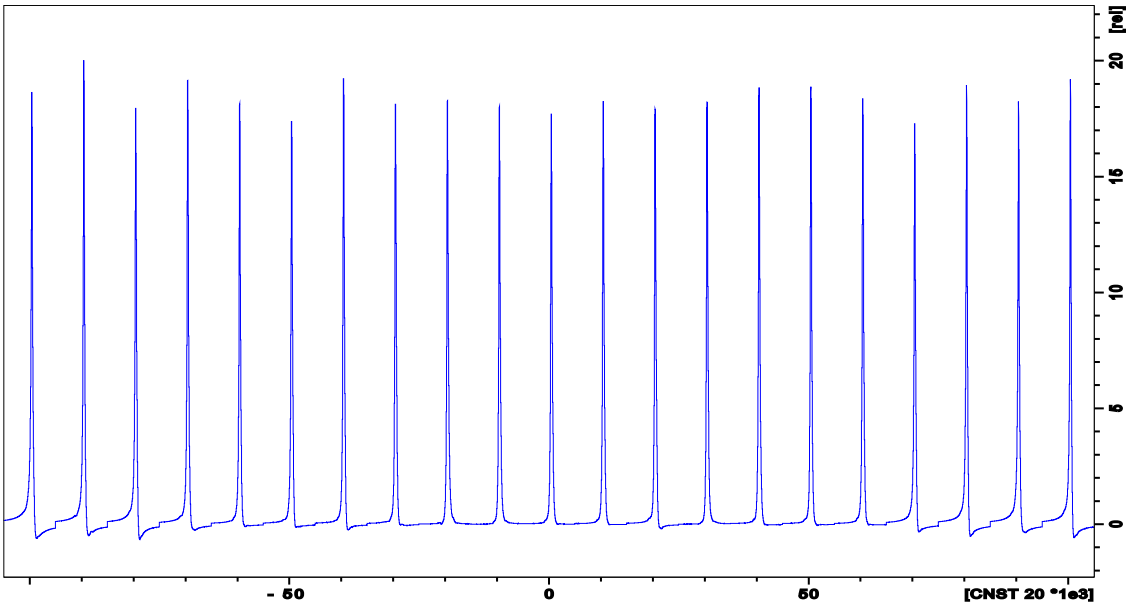

(b) Excitation profile for the simulated R-F-F pulse

Fig. 15. Excitation profiles of residual HDO signal in the mixture of 99.5% D_2O and 0.5% H_2O as sample for the F-R-R and R-F-F **CHORUS** pulses. The offset frequency is varied over 200 *kHz* in the increment of 10 *kHz* ($[-100, 100]$) along *x*– axis and the *y*– axis denotes the intensity of the spectrum.

$$\frac{1}{2a}\left[\int_{-C}^{\omega_0-A_2}\left((\omega_0-\omega)+\frac{1}{2}\frac{A_2^2}{(\omega_0-\omega)}\right)d\omega + \int_{\omega_0-A_2}^{\omega_0+A_2}\omega'_{eff}(\omega)d\omega + \int_{\omega_0+A_2}^{C}\left((\omega-\omega_0)+\frac{1}{2}\frac{A_2^2}{(\omega-\omega_0)}\right)d\omega\right], \tag{59}$$

and the third term is

$$-\frac{1}{a}\left[\int_{\omega_0-\beta A_1}^{\omega_0-A_2}\omega_{eff}(\omega)d\omega + \int_{\omega_0-A_2}^{-C}\left((\omega-\omega_0)+\frac{1}{2}\frac{A_1^2}{(\omega-\omega_0)}\right)d\omega\right]. \tag{60}$$

First considering the linear terms $(\omega_0-\omega)$ of (58), (59) and (60), and omitting the terms which gives no dispersion, obtains

$$\frac{1}{2a}\int_{-C}^{\omega_0-A_2}(\omega_0-\omega)d\omega - \frac{1}{2a}\int_{\omega_0+A_2}^{C}(\omega-\omega_0)d\omega. \tag{61}$$

Adding $\frac{1}{2a}\int_{\omega_0-A_2}^{\omega_0+A_2}(\omega-\omega_0)d\omega$ to (61) as it contributes nothing to the expression obtains the linear term as

$$\frac{1}{2a}\int_{-C}^{C}(\omega_0-\omega)d\omega. \tag{62}$$

Integration of (62) results in $\frac{\omega_0 T}{2}$ which indicates the free-evolution for the time period of $\frac{T}{2}$ in the forward chirp mechanism of refocussing. Hence, the introduced free-evolution compensates the phase dispersion due to the linear terms of the refocussing pulses. The non-linear terms from (58) and (59) cancels each other effect and the remaining term is

$$-\frac{1}{2a}\int_{\omega_0-A_2}^{-C}\frac{A_1^2}{(\omega_0-\omega)}d\omega. \tag{63}$$

Integration of (63) results in the phase dispersion as the function of offset frequency as

$$\Phi(\omega_0)=\frac{A_1^2}{2a}\ln\left(\frac{C+\omega_0}{A_2}\right), \tag{64}$$

Hence, the maximum phase dispersion in (64) due to $\omega_0 = B$ to $\omega_0 = -B$ is

$$\Phi_{max}=\frac{A_1^2}{2a}\ln\left(\frac{1-B/C}{1+B/C}\right).$$

Hence, for each case, the phase dispersion due to the linear first-order terms in the expression of $\Phi(\omega_0)$ can be reduced by adding a free-evolution for time-period $\frac{T}{2}$. The higher-order terms due to the refocussing pulses eliminate each other's effect. A significantly less amount of phase dispersion is present, which depends upon the strength of the excitation pulse (A_1), sweep rate (a), and the chirp pulse sweep parameters B and C. Considering comparatively lower amplitude of the excitation pulse, A_1 and high sweep rate a reduces the maximum phase dispersion. The maximum phase dispersion can be minimized considering $B \ll C$.

3. Simulation results

For the composite pulses shown in Fig. 6 and Fig. 7, the amplitude of the excitation $\frac{\pi}{2}$ pulse is 1 *kHz* and first refocussing π pulse is $\frac{5}{\sqrt{2}}$ *kHz* with sweep rate $2.77\times(2\pi\ kHz)^2$ and amplitude of the last refocussing π pulse is 5 *kHz* with the double sweep rate. For the composite pulses of Fig. 8 and 9 the first refocussing π pulse is 5 *kHz* with sweep rate $2\times2.77\times(2\pi\ kHz)^2$ and amplitude of the last refocussing π pulse is $\frac{5}{\sqrt{2}}$ *kHz* with the sweep rate $2.77\times(2\pi\ kHz)^2$. The offset bandwidth $B/2\pi = 50$ *kHz* and the bandwidth for the tapered end chirp is $C/2\pi = 60$ *kHz*. The time-period T is 43.3213 *ms* and the total duration of the pulse is 129.9639 *ms*. Fig. 10–13 show the evolution of the final state of the magnetizing vector as the function of offset resonance frequency in Fig. 6–9 respectively.

4. Experiment results

Experiment is done on **BRUKER** 750 MHz NMR spectrometer with the mixture of 99.5% D_2O and 0.5% H_2O as the sample. Fig. 14 and 15 show the excitation profiles of the residual HDO signal as a function of the resonance offset. The offset is varied over the range 200 *kHz* ($[-100, 100]$) in the increment of 10 *kHz* around the proton resonance at 4.7 *ppm*. The total time-period for each cycle is 32.49 *ms*. The excitation profile is uniform over the active bandwidth. Fig. 14a, 14b,15a and 15b shows the excitation profile for the pulse in Fig. 6–9 respectively.

5. Conclusion

In this paper, we have studied several combinations of the composite pulse, **CHORUS** for broadband excitation. The composite pulse **CHORUS** is the combination of one chirp excitation pulse and two refocussing chirp inversion pulses, where each of the pulses can take the form of a forward and reverse chirp pulse. The forward sweep pulse starts rotation from the angle $\theta(t) = 0$ to $\theta(t) = \pi$, whereas, the reverse sweep pulse changes the direction of rotation from $\theta(t) = \pi$ to $\theta(t) = 0$, where $\theta(t)$ is the angle of rotation of the rotating frame. Refocussing the magnetization vector is possible if both the inversion pulse are of the same sweep order. The sweep direction of the excitation pulse and the inversion pulse can differ. However, for the different sweep directions of excitation and inversion pulse, the sweep rate of the immediate inversion pulse after the excitation pulse must have the double sweep rate of the excitation pulse to obtain the result. For the amplitude of the inversion pulses, the pulse with a faster sweep rate must have the larger amplitude, which is $\sqrt{2}$ times the pulse with a slower sweep rate. It is shown in this paper that the phase dispersion for the self-refocussing composite pulse only depends upon the magnitude of the excitation pulse, which is the minimum amplitude among all the chirp pulses. The phase dispersion can be further decreased by selecting the chirp range C much larger than the offset frequency range B. This paper describes an analytical explanation for non-uniform phase dispersion reduction in each combination of composite pulse with simulation and experimental results. The experimental result of the simulated pulse exhibits uniform magnetization over a vast range of resonance frequencies.

Data availability

Data will be made available on request.

Declaration of Competing Interest

The authors declare that they have no known competing financial interests or personal relationships that could have appeared to influence the work reported in this paper.

Acknowledgement

We would like to declare that there are no known conflicts of interest associated with this publication and there has been no sig-

nificant financial support for this work that could have influenced its outcome.

References

[1] T.E. Skinner, T.O. Reiss, B. Luy, N. Khaneja, S.J. Glaser, Application of optimal control theory to the design of broadband excitation pulses for high-resolution nmr, J. Magn. Reson. 163 (2003) 8–15, https://doi.org/10.1016/S1090-7807(03)00153-8.

[2] M.R. Koos, H. Feyrer, B. Luy, Broadband excitation pulses with variable rf amplitude-dependent flip angle (radfa), Magn. Reson. Chem. 53 (2015) 886–893, https://doi.org/10.1002/mrc.4297.

[3] T.E. Skinner, K. Kobzar, B. Luy, M.R. Bendall, W. Bermel, N. Khaneja, S.J. Glaser, Optimal control design of constant amplitude phase-modulated pulses: Application to calibration-free broadband excitation, J. Magn. Reson. 179 (2006) 241–249, https://doi.org/10.1016/J.JMR.2005.12.010.

[4] K. Kobzar, T.E. Skinner, N. Khaneja, S.J. Glaser, B. Luy, Exploring the limits of broadband excitation and inversion: Ii. rf-power optimized pulses, J. Magn. Reson. 194 (2008) 58–66, https://doi.org/10.1016/J.JMR.2008.05.023.

[5] N. Khaneja, R. Brockett, S.J. Glaser, Time optimal control in spin systems, Phys. Rev. A - Atomic, Mol. Opt. Phys. 63 (2001) 1–13, https://doi.org/10.1103/PhysRevA.63.032308.

[6] N. Khaneja, A. Dubey, H.S. Atreya, Ultra broadband nmr spectroscopy using multiple rotating frame technique, J. Magn. Reson. 265 (2016) 117–128, https://doi.org/10.1016/J.JMR.2016.02.006.

[7] J. Baum, R. Tycko, A. Pines, Broadband and adiabatic inversion of a two-level system by phase-modulated pulses (1985).

[8] E. Kupce, R. Freeman, Stretched adiabatic pulses for broadband spin inversion, J. Magn. Reson., Series A 117 (1995) 246–256, https://doi.org/10.1006/JMRA.1995.0750.

[9] T.L. Hwang, P.C.V. Zijl, M. Garwood, Broadband adiabatic refocusing without phase distortion, J. Magn. Reson. 124 (1997) 250–254, https://doi.org/10.1006/JMRE.1996.1049.

[10] M. Garwood, L. DelaBarre, The return of the frequency sweep: Designing adiabatic pulses for contemporary nmr, J. Magn. Reson. 153 (2001) 155–177, https://doi.org/10.1006/jmre.2001.2340.

[11] K.E. Cano, M.A. Smith, A.J. Shaka, Adjustable, broadband, selective excitation with uniform phase, J. Magn. Reson. 155 (2002) 131–139, https://doi.org/10.1006/JMRE.2002.2506.

[12] R. Eriks Kupše, Freeman, Wideband excitation with polychromatic pulses, J. Magn. Reson., Series A 108 (1994) 268–273, https://doi.org/10.1006/JMRA.1994.1123.

[13] V.L. Ermakov, J.M. Böhlen, G. Bodenhausen, Improved schemes for refocusing with frequency-modulated chirp pulses, J. Magn. Reson., Series A 103 (1993) 226–229, https://doi.org/10.1006/JMRA.1993.1158.

[14] J.M. Bohlen, M. Rey, G. Bodenhausen, Refocusing with chirped pulses for broadband excitation without phase dispersion, J. Magn. Reson. 84 (1989) (1969) 191–197, https://doi.org/10.1016/0022-2364(89)90018-8.

[15] J.M. Böhlen, I. Burghardt, M. Rey, G. Bodenhausen, Frequency-modulated "chirp" pulses for broadband inversion recovery in magnetic resonance, J. Magn. Reson. 90 (1990) (1969) 183–191, https://doi.org/10.1016/0022-2364(90)90377-L.

[16] J.M. Böhlen, G. Bodenhausen, Experimental aspects of chirp nmr spectroscopy, J. Magn. Reson., Series A 102 (1993) 293–301, https://doi.org/10.1006/JMRA.1993.1107.

[17] N. Khaneja, Chirp mixing, Chem. Phys. Lett. 704 (2018) 62–67, https://doi.org/10.1016/j.cplett.2018.05.047.

[18] M.H. Levitt, Symmetrical composite pulse sequences for nmr population inversion. i. compensation of radiofrequency field inhomogeneity, J. Magn. Reson. 48 (1982) (1969) 234–264, https://doi.org/10.1016/0022-2364(82)90275-X.

[19] M.H. Levitt, R.R. Ernst, Composite pulses constructed by a recursive expansion procedure, J. Magn. Reson. 55 (1983) (1969) 247–254, https://doi.org/10.1016/0022-2364(83)90236-6.

[20] M.H. Levitt, Composite pulses, Prog. Nucl. Magn. Reson. Spectrosc. 18 (1986) 61–122, https://doi.org/10.1016/0079-6565(86)80005-X.

[21] A.J. Shaka, A. Pines, Symmetric phase-alternating composite pulses, J. Magn. Reson. 71 (1987) (1969) 495–503, https://doi.org/10.1016/0022-2364(87)90249-6.

[22] S. Odedra, S. Wimperis, Use of composite refocusing pulses to form spin echoes, J. Magn. Reson. 214 (2012) 68–75, https://doi.org/10.1016/J.JMR.2011.10.006.

[23] S. Odedra, M.J. Thrippleton, S. Wimperis, Dual-compensated antisymmetric composite refocusing pulses for nmr, J. Magn. Reson. 225 (2012) 81–92, https://doi.org/10.1016/J.JMR.2012.10.003.

[24] R. Freeman, S.P. Kempsell, M.H. Levitt, Radiofrequency pulse sequences which compensate their own imperfections, J. Magn. Reson. 38 (1980) (1969) 453–479, https://doi.org/10.1016/0022-2364(80)90327-3.

[25] J.B. Verstraete, W.K. Myers, M. Foroozandeh, Chirped ordered pulses for ultra-broadband esr spectroscopy, J. Chem. Phys. 154 (2021), https://doi.org/10.1063/5.0038511.

[26] J.E. Power, M. Foroozandeh, R.W. Adams, M. Nilsson, S.R. Coombes, A.R. Phillips, G.A. Morris, Increasing the quantitative bandwidth of nmr measurements, Chem. Commun. 52 (2016) 2916–2919, https://doi.org/10.1039/c5cc10206e.

[27] S. Das, J. Jacob, N. Khaneja, Mechanism of chirp excitation, J Magn. Reson. Open 10–11 (2022) 100026, https://doi.org/10.1016/j.jmro.2021.100026.

[28] N. Khaneja, Chirp excitation, J. Magn. Reson. 282 (2017) 32–36, https://doi.org/10.1016/j.jmr.2017.07.003.

[29] S. Sarkar, R.N. Purusottam, A. Kumar, N. Khaneja, Chirp pulse sequences for broadband pi rotation, J. Magn. Reson. 328 (2021) 107002, https://doi.org/10.1016/J.JMR.2021.107002.